

1 ***Bradyrhizobium diazoefficiens* USDA110 nodulation of *Aeschynomene afraspera* is**  
2 **associated with atypical terminal bacteroid differentiation and suboptimal symbiotic**  
3 **efficiency**

4  
5 Running title: *Bradyrhizobium* differentiation in *Aeschynomene*

6  
7 Quentin Nicoud<sup>1\*</sup>, Florian Lamouche<sup>1\*</sup>, Anaïs Chaumeret<sup>1</sup>, Thierry Balliau<sup>2</sup>, Romain Le Bars<sup>1</sup>,  
8 Mickaël Bourge<sup>1</sup>, Fabienne Pierre<sup>1</sup>, Florence Guérard<sup>3</sup>, Erika Sallet<sup>4</sup>, Solenn Tuffigo<sup>1</sup>, Olivier  
9 Pierre<sup>1</sup>, Yves Dessaux<sup>1</sup>, Françoise Gilard<sup>3</sup>, Bertrand Gakière<sup>3</sup>, Istvan Nagy<sup>5,6</sup>, Attila Kereszt<sup>5,6</sup>,  
10 Michel Zivy<sup>2</sup>, Peter Mergaert<sup>1</sup>, Benjamin Gourion<sup>4</sup>, Benoit Alunni<sup>1#</sup>

11  
12 <sup>1</sup> Université Paris-Saclay, CEA, CNRS, Institute for Integrative Biology of the Cell (I2BC),  
13 Gif-sur-Yvette, 91198, France

14 <sup>2</sup> PAPPSO, GQE-Le Moulon, INRAE, CNRS, AgroParisTech, Paris-Saclay University, 91190  
15 Gif-sur-Yvette, France

16 <sup>3</sup> SPOMics platform, Institute of Plant Sciences Paris-Saclay (IPS2), CNRS, INRAE,  
17 Universities Paris-Saclay, Evry and de Paris, Batiment 630, 91405 Orsay, France

18 <sup>4</sup> LIPM, Université de Toulouse, INRAE, CNRS, Castanet-Tolosan, France

19 <sup>5</sup> Institute of Biochemistry, Hungarian Academy of Sciences, Biological Research Centre, 6726  
20 Szeged, Hungary

21 <sup>6</sup> Seqomics Biotechnology Ltd., 6782 Mórahalom, Hungary

22  
23 \* co-first authors

24 # Author to whom correspondence should be addressed: [benoit.alunni@i2bc.paris-saclay.fr](mailto:benoit.alunni@i2bc.paris-saclay.fr)

25  
26  
27  
28  
29  
30  
31  
32  
33

34 **Abstract** (max. 250 words)

35 Legume plants can form root organs called nodules where they house intracellular symbiotic  
36 rhizobium bacteria. Within nodule cells, rhizobia differentiate into bacteroids, which fix  
37 nitrogen for the benefit of the plant. Depending on the combination of host plants and rhizobial  
38 strains, the output of rhizobium-legume interactions is varying from non-fixing associations to  
39 symbioses that are highly beneficial for the plant. *Bradyrhizobium diazoefficiens* USDA110  
40 was isolated as a soybean symbiont but it can also establish a functional symbiotic interaction  
41 with *Aeschynomene afрасpera*. In contrast to soybean, *A. afрасpera* triggers terminal bacteroid  
42 differentiation, a process involving bacterial cell elongation, polyploidy and membrane  
43 permeability leading to loss of bacterial viability while plants increase their symbiotic benefit.  
44 A combination of plant metabolomics, bacterial proteomics and transcriptomics along with  
45 cytological analyses was used to study the physiology of USDA110 bacteroids in these two  
46 host plants. We show that USDA110 establish a poorly efficient symbiosis with *A. afрасpera*,  
47 despite the full activation of the bacterial symbiotic program. We found molecular signatures  
48 of high level of stress in *A. afрасpera* bacteroids whereas those of terminal bacteroid  
49 differentiation were only partially activated. Finally, we show that in *A. afрасpera*, USDA110  
50 bacteroids undergo an atypical terminal differentiation hallmarked by the disconnection of the  
51 canonical features of this process. This study pinpoints how a rhizobium strain can adapt its  
52 physiology to a new host and cope with terminal differentiation when it did not co-evolve with  
53 such a host.

54

55 **Importance** (max 150 words)

56 Legume-rhizobium symbiosis is a major ecological process in the nitrogen cycle,  
57 responsible for the main input of fixed nitrogen in the biosphere. The efficiency of this  
58 symbiosis relies on the coevolution of the partners. Some legume plants, but not all, optimize

59 their return-on-investment in the symbiosis by imposing on their microsymbionts a terminal  
60 differentiation program that increases their symbiotic efficiency but imposes a high level of  
61 stress and drastically reduce their viability. We combined multi-omics with physiological  
62 analyses to show that the non-natural symbiotic couple formed by *Bradyrhizobium*  
63 *diazoefficiens* USDA110 and *Aeschynomene afraspera* is functional but displays a low  
64 symbiotic efficiency associated to a disconnection of terminal bacteroid differentiation features.

## 65 **Introduction**

66 Nitrogen availability is a major limitation for plant development in many environments,  
67 including agricultural settings. To overcome this problem and thrive on substrates presenting a  
68 low nitrogen content, crops are heavily fertilized, causing important environmental damage and  
69 financial drawbacks<sup>1,2</sup>. Plants of the legume family acquired the capacity to form symbiotic  
70 associations with soil bacteria, the rhizobia, which fix atmospheric nitrogen for the plants'  
71 benefit. These symbiotic associations lead to the development of rhizobia-housing root organs  
72 called nodules. In these nodules, the rhizobia adopt an intracellular lifestyle and differentiate  
73 into bacteroids that convert atmospheric dinitrogen into ammonia and transfer it to the plant.  
74 Critical recognition steps occur all along the symbiotic process and define the compatibility of  
75 the plant and bacterial partners<sup>3</sup>. While the mechanisms involved at the early stages of the  
76 symbiosis are well described, those of the later stages are much less clear and might affect not  
77 only the ability to interact but also the efficiency of the symbiosis (ie. the plant benefit).

78 Nodule-specific Cysteine-Rich (NCR) antimicrobial peptides produced by legumes of the  
79 Dalbergioids and Inverted Repeat Lacking Clade (IRLC) were proposed to play a crucial role  
80 in the control of host-symbiont specificity at the intracellular stage of the symbiosis<sup>4</sup>. NCR  
81 peptides are targeted to the bacteroids where they govern the bacteroid differentiation<sup>5-9</sup>. In  
82 these legumes, the differentiation process entails such profound changes that they suppress the  
83 bacteroids' capacity to resume growth and is therefore referred to as terminal bacteroid  
84 differentiation (TBD). TBD contrasts with bacteroid formation in legumes that lack NCR genes  
85 (eg. soybean), where bacteroids are in a reversible state and can resume growth when released  
86 from nodules<sup>10</sup>. Specifically, TBD is associated with cell elongation, an increase in bacteroid  
87 DNA content through a cell cycle switch toward endoreduplication<sup>6,9,11</sup>. Furthermore, an  
88 increased permeability of the bacteroid envelope also occurs during TBD, most probably due  
89 to the interaction of NCR peptides with bacterial membranes<sup>6,7,10,12</sup>. Together, these alterations

90 of bacteroid physiology are associated to a strongly decreased viability of the differentiated  
91 bacteria, that fail to recover growth when extracted from nodules<sup>6</sup>.

92 While many rhizobia have a narrow host range, some species can nodulate a large array of  
93 plant species. One of them, *Bradyrhizobium diazoefficiens* USDA110, can trigger functional  
94 nodules without TBD on soybean (*Glycine max*), cowpea (*Vigna unguiculata*) or siratro  
95 (*Macroptilium atropurpureum*) (Fig 1A-B)<sup>13</sup>. In addition to these species, USDA110 induces  
96 also functional nodules on the TBD-inducing legume *Aeschynomene afraspera* (Fig. 1A-C)<sup>14,15</sup>.  
97 However, in *A. afraspera*, USDA110 shows only very limited features that are usually  
98 associated with TBD, suggesting that the bacterium might be resistant to the TBD process<sup>16</sup>.

99 Herein, we further characterized the bacteroid differentiation in the symbiosis between  
100 USDA110 and *A. afraspera*. Our observations, supported by whole-nodule metabolome  
101 analysis, indicate that USDA110 is poorly matched for nitrogen fixation with *A. afraspera*. To  
102 understand better the adaptation of *B. diazoefficiens* physiology to the *G. max* and *A. afraspera*  
103 nodule environment, we used a combination of transcriptomics (RNA-seq) and shotgun  
104 proteomics (LC-MS/MS) approaches. Finally, we find that USDA110 undergoes a terminal but  
105 atypical bacteroid differentiation in *A. afraspera* with a reduced cell viability and an increased  
106 membrane permeability, while cell size and ploidy level remain unchanged.

107

## 108 **Results**

### 109 ***B. diazoefficiens* USDA110 is poorly matched with *A. afraspera* for nitrogen fixation**

110 Previous reports indicate that *B. diazoefficiens* USDA110, the model symbiont of soybean,  
111 is able to establish a functional nitrogen-fixing symbiosis with *A. afraspera*, a phylogenetically  
112 distant host belonging to the Dalbergioid clade, which naturally interacts with photosynthetic  
113 rhizobia such as *Bradyrhizobium* sp. ORS285 (Fig. 1A-C)<sup>14-18</sup>. To evaluate the efficiency of  
114 this symbiosis, nitrogenase activity of USDA110- and ORS285-infected plants and their

115 nitrogen content were determined. Although nitrogenase activity was detected in both types of  
116 nodules, it was significantly lower in USDA110-nodulated plants (Fig. 1D). A similar trend is  
117 observed for mass gain per nodule mass although this difference is not significant (Fig. 1E).  
118 Nitrogen and carbon contents seemed also reduced in USDA110-nodulated plants as compared  
119 to ORS285-nodulated plants, reaching levels similar to those of non-inoculated plants (Fig. S1).  
120 Accordingly, ORS285-nodulated *A. afraspera* plants display darker green leaves than those  
121 interacting with USDA110.

122 Moreover, their shoot/root mass ratio, a metrics that reflects the nutritional status of the  
123 plant, is reduced in USDA110-nodulated *A. afraspera* plants as compared to ORS285-  
124 nodulated plants, indicating that the plant nutritional needs are not fulfilled (Fig. S2)<sup>19</sup>. To  
125 characterize further this suboptimal symbiosis, we analyzed the whole-nodule metabolome.  
126 Soybean nodules infected with USDA110 were used as a reference (Fig. S3). Allantoin, which  
127 is known to be the major nitrogen form exported from soybean nodules, is specifically detected  
128 in them (Fig. 1F)<sup>20</sup>. On the contrary, asparagine and glutamine are the principal exported  
129 nitrogen compounds in *A. afraspera* nodules and their amount is lower in USDA110-infected  
130 nodules as compared to ORS285-infected nodules, indicating a reduced nitrogen fixation by the  
131 bacteroids (Fig. 1F)<sup>18</sup>.

132 In addition, we find specifically in USDA110-infected *A. afraspera* nodules the  
133 accumulation of sucrose, phosphoric acid and ascorbate, and oppositely, a strong reduction in  
134 the trehalose content (Fig. 1F, Fig. S3). Sucrose derived from phloem sap is metabolized in  
135 nodules to fuel the bacteroids with carbon substrates, usually dicarboxylates. The accumulation  
136 of sucrose in nodules indicates a symbiotic dysfunction. Also, the accumulation of phosphoric  
137 acid in nodules suggests that nitrogen fixation is not reaching its optimal rate. Ascorbate has  
138 been shown to increase nitrogen fixation activity by modulating the redox status of  
139 leghemoglobin<sup>21,22</sup>. Thus, its accumulation in nodules with reduced nitrogen fixation capacity

140 could be a stress response to rescue nitrogen fixation in nodules that do not fix nitrogen  
141 efficiently. A trehalose biosynthesis gene is upregulated in ORS285 bacteroids in *A. afraspera*,  
142 suggesting that TBD is accompanied by the synthesis of this osmo-protectant disaccharide<sup>17</sup>.  
143 The lower synthesis in USDA110 bacteroids suggests an altered TBD. Together these data  
144 indicate a metabolic disorder in the USDA110-infected nodules, in agreement with USDA110  
145 being a suboptimal symbiont of *A. afraspera*.

146

### 147 **Overview of the USDA110 bacteroid proteomes and transcriptomes**

148 In order to better understand the poor interaction between USDA110 and *A. afraspera*, the  
149 bacteroid physiology was analyzed through transcriptome and proteome analysis. The efficient  
150 soybean bacteroids and the free-living USDA110 cells cultivated in rich medium (exponential  
151 growth phase in aerobic condition) were used as references (Fig. 2A).

152 Prior to quantification of transcript abundance or identification and quantification of protein  
153 accumulation, the transcriptome dataset was used to re-annotate the USDA110 genome with  
154 the EugenePP pipeline<sup>23</sup>. This allowed the definition of 876 new CDS, ranging from 92 to  
155 1091bp (median size = 215bp or 71.6 aa) with 11.5% of them having a predicted function or at  
156 least a match using InterProScan (IPR). This extends the total number of CDS in the USDA110  
157 genome to 9171. Moreover, we also identified 246 ncRNAs, ranging from 49 to 765 bp (median  
158 = 76 bp), which were not annotated before. Proteomic evidence could be found for 28 new CDS  
159 (3.2% of the new CDS, median size = 97.6 aa). The complete reannotation of the genome is  
160 described in Table S1.

161 In the proteome dataset, 1808 USDA110 proteins were identified. Principal component  
162 analysis (PCA) of all the replicate samples and sample types revealed their partitioning  
163 according to the tested conditions. The first axis of the PCA (40.2% of the observed variance)  
164 separates bacteroid profiles from the exponential culture, whereas the second axis separates *G.*

165 *max* bacteroids from *A. afraspera* bacteroids (14.9% of the observed variance; Fig. 2B). The  
166 samples of the transcriptome datasets are similarly distributed on the PCA plot, with a first axis  
167 explaining 42.6% of the observed variance and a second axis explaining 23.5% of the observed  
168 variance (Fig. 2B).

169 Although differences are less pronounced in the proteome dataset than in the transcriptome  
170 dataset, COG analysis shows similar profiles across functional categories, except for membrane  
171 proteins that are less well identified in proteomics than transcriptomics (Fig. S4). In the  
172 transcriptomic dataset, 3150 genes are differentially expressed in at least one condition  
173 (differentially expressed genes or DEGs). Among the 1808 proteins identified, 815 show  
174 differential accumulation (differentially accumulated proteins or DAPs) and 438 of the cognate  
175 genes are also differentially expressed in the transcriptome datasets, whereas 175 DEGs are not  
176 DAPs (Fig. 2C).

177 We analyzed the Pearson correlation between transcriptomic and proteomic profiles and  
178 found that ~66% of the bacterial functions that show significant differences in both approaches  
179 display a high correlation coefficient ( $r > 0.9$ ) whereas less than 1% of the functions show strong  
180 negative correlation ( $r < -0.9$ ; Fig. 2D). This observation suggests that the transcriptome (which  
181 provides a more exhaustive view than the proteome) and the proteome provide a  
182 complementary picture of bacterial physiology, and they tend to show a congruent information  
183 if we restrict our analysis to the genes with differential accumulation/expression (Fig. 2E).  
184 However, there is still around 66% of the DEGs, which were detected by the proteomic analysis,  
185 that are not DAPs. Our description of the bacterial functions will be primarily based on the  
186 functions that are both DEGs and DAPs, as there is stronger evidence of their modulation in the  
187 tested conditions. The transcriptome alone will be used only when proteomics is not  
188 informative, for example to analyze regulons and stimulons that have been described previously  
189 in USDA110.



190

191 **Symbiotic functions common to both types of USDA110 bacteroids**

192 Among the 815 DAPs, 705 and 699 proteins are significantly differentially accumulated in  
193 *G. max* and *A. afraspera* respectively compared to the bacterial culture control. Strikingly, 646  
194 proteins are commonly differentially accumulated in both plant nodules (Table S1).

195 In the transcriptomic dataset, 1999 DEGs, representing ~21% of the genome, were  
196 identified between the bacterial culture and the bacteroids, regardless of the host. Among them,  
197 1076 genes displayed higher expression in nodules (including seven newly annotated ncRNAs  
198 and one newly annotated CDS among the 20 differentially expressed genes with highest fold  
199 change) and 923 genes were repressed *in planta* (including two newly annotated ncRNAs and  
200 two newly annotated CDS among the 20 DEG with highest fold change, Table S1).

201 Restricting the analysis to the bacterial functions that are both differentially expressed  
202 (DEG) and differentially accumulated (DAP) *in planta* in both hosts as compared to the  
203 bacterial culture identified 222 genes/proteins, 150 being upregulated and 72 being repressed  
204 *in planta* respectively (Fig. 3A). Notably, six newly annotated genes are in this gene list  
205 including one putative regulator (Bd110\_01119) that is induced during symbiosis. Among the  
206 functions commonly DEG and DAP *in planta*, only four functions showed opposite trends in  
207 proteomics and transcriptomics.

208 The proteome and transcriptome data provided a coherent view of the nitrogen fixation  
209 metabolism of *B. diazoefficiens* in the tested conditions. Key enzymes involved in microoxic  
210 respiration and nitrogen fixation were detected amongst the proteins having the highest spectra  
211 number in the nodule samples (Fig. 3A, Table S1) and the corresponding genes are among the  
212 most strongly expressed ones in bacteroids, while almost undetectable in the free-living  
213 condition. This includes for instance, the nitrogenase and the nitrogenase reductase subunits,  
214 which constitute the nitrogenase enzyme complex responsible for nitrogen conversion into

215 ammonia. They belong to a locus of 21 genes from *blr1743* (*nifD*) to *bll1778* (*ahpC\_2*),  
216 including the genes involved in nitrogenase cofactor biosynthesis, in electron transport to  
217 nitrogenase, and in microaerobic respiration, that are among the highest expressed ones in  
218 bacteroids of both host plants, both at the gene and protein expression level. The slightly higher  
219 level of the dinitrogenase reductase NifH detected in proteomics was not supported by western  
220 blot analysis, which showed apparent similar protein level in both bacteroid conditions (Fig.  
221 S5). Strikingly, the two bacteroid types did not show a notable difference in the expression of  
222 these genes and proteins, suggesting that the activation of the nitrogen fixation machinery is  
223 not a limiting factor underlying the suboptimal efficiency of strain USDA110 in *A. afraspera*  
224 nodules.

225 In addition to these expected bacteroid functions, many other proteins were identified that  
226 specifically and strongly accumulated in both nodule types. This is the case of the chaperonins  
227 GroEL1/GroES1, which are strongly upregulated and reach high gene expression and protein  
228 levels in both bacteroids. The upregulation of these chaperonins is remarkable because other  
229 GroEL/GroES (4, 5 and 7) proteins are also very strongly accumulated in a constitutive manner.  
230 This indicates that bacteroids have a high demand for protein folding, possibly requiring  
231 specific GroEL isoforms, a situation reminding the requirement of one out of five GroEL  
232 isoforms for symbiosis in *Sinorhizobium meliloti*, the symbiont of *Medicago sativa*<sup>12,24</sup>.  
233 Another example of a bacteroid-specific function is the hydrogenase uptake system, whose gene  
234 expression was induced in both bacteroid types from nearly no expression in culture.  
235 Hydrogenase subunit HupL\_2 (*bll6941*) was found amongst the proteins displaying the highest  
236 spectra number in the nodule samples suggesting important electron recycling in bacteroids of  
237 the two hosts. Another one is the 1-aminocyclopropane-1-carboxylic acid (ACC) deaminase  
238 (*blr0241*), which was also amongst the most strongly accumulated proteins in nodules and was  
239 significantly less abundant in free-living USDA110. An outer membrane protein (*bll1872*)

240 belonging to the NifA regulon<sup>25</sup> was also strongly induced *in planta*, with a transcript level  
241 among the top 10 genes in *A. afraspera*. Additionally, a locus of seven genes (*blr7916-blr7922*)  
242 encoding an amidase enzyme and a putative peptide transporter composed of two  
243 transmembrane domain proteins, two ATPases and two solute-binding proteins was strongly  
244 upregulated in the two bacteroid types, with three protein being also over-accumulated *in planta*  
245 (Fig. 3A; Table S1).

246 Oppositely, motility genes encoding flagella subunits (*bll5844-bll5846*), metabolic  
247 enzymes and transporter subunits are strongly downregulated during symbiosis and hardly  
248 detectable at the protein level *in planta* (Fig. 3A).

249 Taken together, these data show that both bacteroid types display a typical nitrogen fixation-  
250 oriented metabolism, with a partial shutdown of housekeeping functions. This indicates that  
251 despite the apparent reduced symbiotic efficiency of USDA110 in *A. afraspera* nodules, the  
252 bacterium fully expresses its symbiotic program within this non-native host as it does in  
253 soybean, its original host. Thus, the sub-optimal functioning of the *A. afraspera* nodules does  
254 not seem to come from a bacterial defect to express the symbiotic program, but possibly from  
255 an unfavorable host microenvironment or from a lack of metabolic integration of these  
256 maladapted partners.

257

### 258 **Host-specific functions**

259 Comparison of the *A. afraspera* and *G. max* bacteroids revealed also significant differences  
260 in the proteomes and transcriptomes. At the transcriptomic level, 935 DEGs could be identified  
261 between the two bacteroid types (509 *A. afraspera* > *G. max* and 426 *G. max* > *A. afraspera*).  
262 One notable feature of the transcriptome is the identification of four newly annotated ncRNA  
263 and one new CDS amongst the 20 most induced DEGs in *A. afraspera* nodules and the presence  
264 of five newly annotated CDS amongst the 20 most induced DEGs in *G. max* nodules (Table

265 S1). However, when considering only the functions that display congruent and significant  
266 differences in terms of transcripts and protein levels between plant hosts, we fall down to 63  
267 genes/proteins, 33 being induced in *A. afraspera* nodules and 30 being induced in *G. max*  
268 nodules (Fig. 3B).

269 Interestingly, the phenylacetic acid degradation pathway (PaaABCDEIK, *blr2891-blr2897*)  
270 was highly expressed in *A. afraspera* nodules (although only PaaABCD and PaaK have been  
271 detected by proteomics), as well as a yet uncharacterized cluster of genes putatively involved  
272 in toluene degradation (*blr3675-blr3680*). The chaperone GroEL2 is also specifically induced  
273 in *A. afraspera*. Similarly, three S1 peptidases (Dop: *blr2591*, *blr3130* and *blr7274*) are highly  
274 expressed in the nodules of this latter host together with a RND efflux pump (*bll3903*) and a  
275 LTXXQ motif protein (*bll6433*), a motif also found in the periplasmic stress response CpxP<sup>26</sup>.  
276 The over-accumulation of these proteins suggests that bacteroids are facing stressful conditions  
277 during this interaction with *A. afraspera*. An uncharacterized ABC transporter solute binding  
278 protein (*blr7922*) was also overexpressed in *A. afraspera*.

279 One  $\alpha\beta$  hydrolase (*blr6576*) and a TonB-dependent receptor-like protein (*bll2460*) were  
280 over-accumulated in a *G. max*-specific manner. Similarly, an uncharacterized metabolic cluster  
281 including transketolases (*blr2167-blr2170*), the heme biosynthetic enzyme HemN1 (*bll2007*)  
282 and to a lesser extent an anthranilate phosphoribosyl-transferase (TrpD encoded by *bll2049*)  
283 are overexpressed in soybean nodules.

284

## 285 **USDA110 transcriptomics data in the perspective of previously described regulons** 286 **and stimulons**

287 USDA110 is one of the best-characterized rhizobial strains in terms of transcriptomic  
288 responses to various stimuli as well as the definition of regulons<sup>27</sup>. We analyzed the behavior  
289 of these previously defined gene networks in USDA110 in our dataset (Table S2). To initiate

290 the molecular dialog that leads to nodule formation, plants secrete flavonoids like genistein in  
291 their root exudates, which are perceived by the rhizobia and trigger Nod factor production. At  
292 14 dpi, when the nodule is formed and functioning, the genistein stimulon, which comprises the  
293 NodD1, NodVW, TtsI and LafR regulons, is not anymore activated in bacteroids. The symbiotic  
294 regulons controlled by NifA, FixK1, FixK2, FixLJ and sigma54 (RpoN) were activated *in*  
295 *planta*, indicating that nitrogen fixation was going on in both hosts. Accordingly, the nitrogen  
296 metabolism genes controlled by NtrC were activated *in planta*. Additionally, the PhyR/EcfG  
297 regulon involved in general stress response is not activated in bacteroids. Differences between  
298 hosts were however not observed for any of these regulons/stimulons. The only stimulon that  
299 showed differential expression between hosts is the one involved in aromatic compound  
300 degradation, which was highly expressed in *A. afraspera* nodules. Similar upregulation of the  
301 vanillate degradation pathway was observed in the transcriptome of *Bradyrhizobium* sp.  
302 ORS285 in *A. afraspera* and *A. indica* nodules<sup>17</sup>, suggesting that Dalbergioid hosts display a  
303 higher aromatic compound content in nodules than *G. max*. In line with this hypothesis, some  
304 of the most differentially accumulated sets of proteins (*A. afraspera* > *G. max*) are involved in  
305 the degradation of phenylacetic acid (PaaABCDK and *blI0339*) suggesting that the bacterium  
306 converts phenylalanine (or other aromatic compounds) ultimately to fumarate through this route  
307 (Fig. 3B)<sup>28</sup>. Similarly, enzymes of another pathway involved in phenolic compound degradation  
308 (*blr3675-blr3680*) are accumulated in *A. afraspera* nodules (Fig. 3B, Table S1).

309

310 **Expression pattern of orthologous genes between ORS285 and USDA110 in *A.***  
311 ***afraspera* nodules**

312 In a previous study<sup>17</sup>, a transcriptome analysis was performed on *Bradyrhizobium* sp.  
313 ORS285 in interaction with *A. afraspera* and in culture. *Bradyrhizobium* sp. ORS285 is a strain  
314 that co-evolved with *A. afraspera*, leading to an efficient symbiosis hallmarked by TBD, *id est*

315 cell elongation and polyploidization of the bacteroids. In order to compare gene expression of  
316 these two nodule-forming rhizobia in culture and *in planta*, we determined the set of  
317 orthologous genes between the two strains using the Phyloprofile tool of Mage Microscope  
318 website. This analysis yielded a total of 3725 genes (Table S3). The heatmap on Figure 4A  
319 presents the modulation of gene expression (LFC) between *A. afraspera* nodules and the  
320 bacterial culture for the orthologous genes in each bacterium, regardless of their statistical  
321 significance. When taking  $FDR < 0.01$  in account, we identified sets of genes that are  
322 differentially expressed *in planta* in either bacterium or in both (Fig. 4B).

323 Only 343 genes displayed differential expression ( $FDR < 0.01$  and  $|LFC| > 1.58$ ) *in planta*  
324 in both bacteria as compared to their respective culture control (Fig. 4C). A majority of these  
325 genes (86.8%) exhibited congruent expression patterns. First, the *nif*, *fix* and *hup* genes are  
326 commonly and highly induced in both strains during their symbiotic life with *A. afraspera*, a  
327 hallmark of a functional symbiosis. However, there are differences in their expression level,  
328 with a higher expression of the symbiotic genes in ORS285 (*nifHDK* represent 12.5% of all  
329 reads in *A. afraspera* nodules)<sup>17</sup> than in USDA110 (*nifHDK* represent only 2.5% of all reads in  
330 *A. afraspera* nodules), consistently with a more efficient interaction occurring between ORS285  
331 and *A. afraspera*. Additionally, the Kdp high affinity transport system, the phosphate (*pstCAB*,  
332 *phoU*, *phoE*, *phoC*) and phosphonate metabolism (*phnHIJKL*) are activated *in planta* in both  
333 bacteria (Fig. 4B-C). The stress-marker *dop* protease gene is also induced in both bacteria in *A.*  
334 *afraspera* nodules (Fig. 4C).

335 Additionally, 1026 genes were differentially expressed solely in ORS285, and similarly  
336 there was 604 DEG specific to USDA110 (Fig. 4B). For example, the general secretory pathway  
337 seems to be specifically induced in ORS285<sup>17</sup>. Oppositely, USDA110 displays an induction of  
338 the *rhcJQRU* genes which are involved in the injection of type three effector proteins that can  
339 be important for the establishment of the symbiosis whereas they are not induced or even

340 repressed in ORS285 (Fig. 4B). This is also the case of the nitrite reductase encoding gene *nirK*  
341 (*blr7089/BRAD285\_v2\_0763*; Fig. 4C). In addition, USDA110 induces the expression of an  
342 ACC deaminase (*blr0241*), while its ortholog is repressed in ORS285 (*BRAD285\_v2\_3570*)  
343 during symbiosis (Fig. 4C). Bacterial ACC deaminases can degrade ACC, a precursor of  
344 ethylene, and thereby modulate ethylene levels in the plant host and promote the nodulation  
345 process<sup>29</sup>.

346

347 ***Bradyrhizobium diazoefficiens* USDA110 bacteroids undergo bona fide TBD in**  
348 ***Aeschynomene afraspera* nodules despite very weak morphological and ploidy**  
349 **modifications**

350 In a previous description of the *A. afraspera* - *B. diazoefficiens* USDA110 interaction, the  
351 typical TBD features were not observed and the bacteroids were very similar to those in *G. max*  
352 where no TBD occurs<sup>16</sup>. At the molecular level, accumulation of the replication initiation factor  
353 DnaA is higher in soybean than in *A. afraspera* (Table S1). Similarly, the MurA peptidoglycan  
354 synthesis enzyme (encoded by *bll0822*) that may play a role in cell elongation during TBD was  
355 detected to similar levels in both bacteroids (Table S1). Taken together, the molecular data do  
356 not clearly indicate whether USDA110 bacteroids undergo TBD in *A. afraspera*. Therefore, we  
357 investigated the features of the USDA110 bacteroids in *A. afraspera* nodules in more detail.

358 We analyzed bacteroid differentiation features in USDA110 bacteroids extracted from  
359 soybean and *A. afraspera* nodules. The interaction between *A. afraspera* and *Bradyrhizobium*  
360 sp. ORS285 was used as a positive control for TBD features<sup>9,30,31</sup>. TBD is characterized by cell  
361 elongation. We quantified cell length, width, area and shape of purified bacteroids and culture  
362 controls. Whereas ORS285 bacteroids were enlarged within *A. afraspera* nodules as compared  
363 to their free-living counterparts, USDA110 bacteroids were similar to free-living bacteria in both  
364 soybean and *A. afraspera* (Fig. 5A; Fig. S6). Another feature of TBD is endoreduplication.

365 Analysis of the bacterial DNA content of ORS285 bacteroids in *A. afraspera* by flow cytometry  
366 shows peaks at 6C and more<sup>9</sup>. As expected, USDA110 bacteroids in *G. max* yields only two  
367 peaks, at 1C and 2C, similarly to the cycling cells in the bacterial culture sample (Fig. 5B)<sup>16</sup>.  
368 Strikingly, similar results were obtained for USDA110 in *A. afraspera*. Thus, with respect to  
369 the DNA content and cell size, the USDA110 bacteroids do not display the typical TBD features  
370 in *A. afraspera* nodules. Loss of membrane integrity is a third hallmark of TBD that likely  
371 strongly contributes to the loss of viability of bacteroids. Time-course analysis of propidium  
372 iodide (PI) uptake by bacteroids and the corresponding culture controls were performed to  
373 assess bacteroid permeability (Fig. S7). Twenty minutes after PI application, USDA110  
374 bacteroids from *A. afraspera* display an increased permeability that is much closer to ORS285  
375 bacteroids in interaction with *A. afraspera* than to the low permeability of USDA110 bacteroids  
376 from *G. max* nodules (Fig. 5C). Also the free-living counterparts exhibit a very low  
377 permeability. Taken together, this suggests that the envelope of USDA110 bacteroids is more  
378 permeable in the NCR-producing *A. afraspera* nodules, even if it does not reach the  
379 permeability level of the ORS285 strain. To analyze bacterial viability, bacteroids extracted  
380 from nodules were plated and the colony forming units (cfu) were determined (Fig. 5D). In *G.*  
381 *max*, USDA110 formed  $1.46 \times 10^{10}$  colonies/mg nodule (~100% survival). Oppositely, ORS285  
382 formed only  $5.42 \times 10^7$  colonies/mg nodule in *A. afraspera* (~0.5% survival). Interestingly,  
383 USDA110 formed  $1.13 \times 10^8$  colonies/mg nodule in *A. afraspera* (~1% survival), indicating that,  
384 despite the absence of cell enlargement and endoreduplication USDA110 bacteroids lose their  
385 viability and undergo a *bona fide* terminal differentiation in *A. afraspera*. Thus, in the NCR-  
386 producing plant *A. afraspera*, USDA110 bacteroids display a disconnection of the four  
387 canonical TBD features (ie. cell size, ploidy level, membrane permeability and cell viability).

388

389 **Discussion**



390

391 ***Aeschynomene afraspera* triggers atypical but terminal differentiation of USDA110**  
392 **bacteroids**

393 In a previous study, we noticed that, in *A. afraspera*, USDA110 forms a functional  
394 symbiosis although bacteroids do not display features that are usually associated with TBD<sup>16</sup>.  
395 Here we show that no endoreduplication and cell elongation of USDA110 occur in terminally  
396 differentiated bacteroids that fix nitrogen in a suboptimal way. Accordingly, the protein level  
397 of DnaA, the genome replication initiator, was higher in soybean than in *A. afraspera* bacteroids  
398 and the MurA level was not different between bacteroid conditions, confirming that  
399 polyploidization and cell elongation did not occur in this host. Such unusual terminal bacteroid  
400 differentiation is reminiscent of the bacteroids in *Glycyrrhiza uralensis*. This plant of the IRLC  
401 expresses NCR peptides<sup>11</sup>. However, one of its compatible symbionts, *Sinorhizobium fredii*  
402 strain HH103, does not undergo any loss of viability, no change in DNA content and no cell  
403 elongation<sup>32</sup>, while another symbiont, *Mesorhizobium tianshanense* strain HAMBI 3372  
404 showed all TBD features<sup>33</sup>. The influence of the bacterial genotype on terminal/non-terminal  
405 differentiation of bacteroids was also suggested in *Medicago truncatula* in which, the gene *hrrP*  
406 might confer to some *Sinorhizobium* strains a resistance against the differentiation process  
407 triggered by some *M. truncatula* ecotypes<sup>34</sup>. In these two IRLC plants (ie. *M. truncatula* and *G.*  
408 *uralensis*), bacteria undergo a complete TBD or no TBD at all in a strain-dependent manner,  
409 but there is no clear uncoupling of the features of TBD (cell  
410 elongation/endoreduplication/altered viability) as shown here in the case of *B. diazoefficiens*  
411 USDA110-A. *afraspera*.

412 The surprising differentiation of USDA110 in *A. afraspera* nodules raises questions about  
413 the molecular mechanisms supporting this phenomenon. We consider two possible hypotheses:  
414 strain USDA110 might be more sensitive to the differentiation factors of the host than strain

415 ORS285 and be rapidly “terminally” differentiated, before the other differentiation features,  
416 that are potentially important for symbiotic efficiency, can take place. Alternatively, USDA110  
417 might be resistant to the plant effectors that trigger the elongation and polyploidization features.

418 In agreement with the latter possibility, the application of NCR peptides has very limited  
419 effect on strain USDA110 as compared to *S. meliloti* and to other plant-associated bacteria<sup>16,35</sup>.  
420 NCR insensitivity may be due to the thick hopanoid layer that is present in the outer membrane  
421 of strain USDA110, as the hopanoid biosynthesis mutant *hpnH* is more sensitive to NCR  
422 peptides and shows symbiotic defects in *A. afraspera* but not in *G. max*<sup>36</sup>. Moreover, the altered  
423 peptidoglycan structure in the strain USDA110 DD-carboxypeptidase mutant resulted in an  
424 increased TBD process with endoreduplicated and elongated bacteroids in *A. afraspera*<sup>16</sup>. This  
425 suggests that the envelope of strain USDA110 prevents a canonical TBD to occur. Possibly,  
426 NCR peptides are not able to reach their intracellular targets required to induce  
427 endoreduplication and cell division arrest, while their effect on cell viability through pore  
428 formation and membrane destabilization is still effective.

429 A survey of TBD in the legumes has identified multiple occurrences of the process in several  
430 subclades of the legumes but found that the majority of legumes do not have TBD<sup>37</sup>. The  
431 classification in this study was based on a morphological analysis of the bacteroids. Ancestral  
432 state reconstruction based on this classification suggested that the non-differentiated bacteroids  
433 are ancestral and that TBD evolved at least five times independently in legumes<sup>37</sup>. The  
434 discovery of bacteroids that are terminally differentiated without any obvious morphological  
435 changes opens the possibility that the occurrence of TBD might be underestimated in the  
436 legume family. Similarly, in the IRLC clade, the extent of morphological bacteroid  
437 differentiation was correlated to the size of the cationic NCR peptides repertoire and in legumes  
438 with few NCR peptides, the morphological modification of bacteroids can be minor<sup>11,33</sup>. In  
439 addition, at the molecular level, TBD is originally ascribed to the production of symbiotic

440 antimicrobial peptides, the NCRs, by nodules<sup>7</sup>, but more recently, other types of antimicrobial  
441 peptides such as the NCR-like, GRP, MBP1 and CAPE peptides specifically produced in  
442 nodules of different plants were proposed to contribute to bacteroid differentiation<sup>9,38-40</sup>. Thus,  
443 if TBD would indeed be more widespread than currently estimated on the basis of  
444 morphological bacteroid features, the currently proposed evolutionary scenario of bacteroid  
445 formation might require revision.

446

#### 447 **Terminal differentiation is associated with specific stress response**

448 The TBD of strain USDA110 in *A. afraspera* is associated with a higher accumulation of  
449 stress markers compared to the *G. max* bacteroids. These markers include four proteases (Dop,  
450 Lon\_2, *blr3130* and *blr7274*) and one chaperonin (GroEL\_2). Similar induction of proteases  
451 and chaperonins have been reported in NCR-treated *S. meliloti* cultures<sup>35</sup>, indicating that this  
452 response may be linked to the perception of *A. afraspera* NCR-like peptides in USDA110.

453 The genes encoding these stress related proteins are not part of the well-characterized  
454 general stress response (GSR) controlled by the PhyR/EcfG signaling cascade in *B.*  
455 *diazoefficiens* USDA110<sup>41</sup>. On the other hand, we found that the PhyR/EcfG regulon in  
456 USDA110 is not activated in the bacteroids of both host plants (Table S2). This observation  
457 contrasts with our previous study of *Bradyrhizobium* sp. ORS285 transcriptome during  
458 symbiosis with *Aeschynomene* plants, which showed that the PhyR/EcfG cascade was  
459 upregulated *in planta*<sup>17</sup>. Nevertheless, the expression of the Dop protease was induced in *A.*  
460 *afraspera* in both bacteria (Fig. 4C). Together, the omics data suggest that bacteroids of  
461 *Bradyrhizobium* spp. activate stress-related genes in the TBD-inducing *A. afraspera* host but  
462 differences exist in the activation of specific stress responses at the strain level.

463

464 **Correlation between bacteroid differentiation features and symbiotic efficiency for the**  
465 **plant**

466 TBD is associated with the massive production of symbiotic antimicrobial peptides such as  
467 NCR, NCR-like and CAPE peptides in different plants<sup>5,9,38,40</sup>. They represent ~10% of the  
468 nodule transcriptomes in *M. truncatula* (analysis of the data from ref 42) and their production  
469 is thus potentially a strong energetic cost for the plant, raising questions about the benefits of  
470 the TBD process. TBD appeared independently in different legume clades<sup>9,37</sup>, suggesting that  
471 plants imposing this process obtain an advantage which might be a higher symbiotic benefit.  
472 Increased symbiotic efficiency has indeed been observed in hosts imposing TBD<sup>17,43,44</sup>. The  
473 findings reported here, comparing bacteroids and symbiotic efficiency in *A. afraspera* infected  
474 with strain ORS285 and strain USDA110, are in agreement with this hypothesis. Also in the  
475 symbiosis of *M. truncatula* in interaction with different *S. meliloti* strains, a similar correlation  
476 was observed between the level of bacteroid differentiation and the plant growth stimulation<sup>45</sup>.  
477 However, the simultaneous analysis of the bacteroid differentiation and symbiotic performance  
478 of an extended set of *Aeschynomene-Bradyrhizobium* interactions has shown that, perhaps not  
479 unexpectedly, the symbiotic efficiency of the plant-bacterium couple is not solely correlated  
480 with bacteroid differentiation and that other factors can interfere with the symbiotic efficiency  
481 as well<sup>46</sup>.

482

483 **Conclusion**

484 *Bradyrhizobium diazoefficiens* USDA110 is a major model in the legume-rhizobium  
485 symbiosis, mainly thanks to its interaction with *G. max*, the worldwide most cultivated legume.  
486 Although omic studies have been conducted in this strain in symbiosis with various hosts<sup>13,25</sup>,  
487 this is the first time that this bacterium is studied at the molecular level in symbiosis with a  
488 NCR-producing plant that normally trigger a typical terminal bacteroid differentiation in its

489 symbionts. The symbiosis between USDA110 and *A. afraspera* is functional even if nitrogen  
490 fixation and plant benefits are sub-optimal.

491 Terminal bacteroid differentiation is taking place in the NCR-producing host *A. afraspera*,  
492 as bacterial viability is impaired in USDA110 bacteroids, whereas morphological changes and  
493 the cell cycle switch to endoreduplication are not observed. We also show by combining  
494 proteomics and transcriptomics that the bacterial symbiotic program is expressed in *A.*  
495 *afraspera* nodules in a similar way as in *G. max*, although host-specific patterns were also  
496 identified. However, the bacterium is under stressful conditions in the *A. afraspera* host,  
497 possibly due to the production of NCR-like peptides in this plant. Integration of datasets from  
498 different bacteria in symbiosis with a single host, like ORS285 and USDA110 in symbiosis  
499 with *A. afraspera*, shed light on the differences in the stress responses activated in *A. afraspera*  
500 and confirmed that the symbiosis is functional but suboptimal in this interaction. The molecular  
501 data presented here provide a set of candidate functions that could be analyzed for their  
502 involvement in the adaptation to a new host and to the TBD process.

## 503 **Material and Methods**

### 504 **Bacterial cultures and bacteroid extraction**

505 *B. diazoefficiens* USDA110<sup>47</sup> and *Bradyrhizobium* sp. ORS285 were cultivated in YM  
506 medium at 30°C in a rotary shaker<sup>48</sup>. For transcriptomic analysis, culture samples (OD<sub>600nm</sub> =  
507 0.5) were collected and treated as in Chapelle et al. (2015)<sup>49</sup>.

508 *G. max* ecotype Williams 82 and *A. afraspera* seeds were surface-sterilized and the plants  
509 were cultivated and infected with rhizobia for nodule formation as described in Barrière et al.  
510 (2017)<sup>16</sup>. Nodules were collected at 14 days post inoculation (dpi), immediately immersed in  
511 liquid nitrogen and stored at -80°C until use. Each tested condition (in culture and *in planta*)  
512 was produced in biological triplicates.

513

## 514 **Phylogeny analysis**

515 Nucleotide sequence of *matK* genes were collected on NCBI using accession numbers  
516 described in references 50 and 51 and analyzed on phylogeny.fr ([www.phylogeny.fr](http://www.phylogeny.fr)). They  
517 were aligned using ClustalW with manual corrections, before running a phyML (GTR - Gamma  
518 model) analysis with 500 bootstraps. A Bayesian inference tree was also generated (GTR + G  
519 + I) and provided similar topology as the maximum likelihood tree (data not shown). Trees  
520 were visualized and customized using TreeDyn.

521

## 522 **Genome annotation and RNA-seq analysis**

523 Nodule and bacterial culture total RNA was extracted and treated as previously described  
524 in <sup>17</sup>. Oriented (strand-specific) libraries were produced using the SOLiD Total RNA-seq kit  
525 (Life Technologies) and were sequenced on a SOLiD 3 station yielding ~40 million 50bp single  
526 reads. Trimming and normalization of the reads were performed using the CLC workbench  
527 software. Subsequently, the reads were used to annotate the genome using EugenePP<sup>23</sup>, and the  
528 mapping was performed using this new genome annotation. Analysis of the transcriptome using  
529 DE-seq2 and data representation were performed as previously described<sup>17</sup>. Differentially  
530 expressed genes (DEG) showed an absolute  $\log_2$  fold change (|LFC|) > 1.58 (ie. fold change >  
531 3) with a false discovery rate (FDR) < 0.01.

532

## 533 **Proteomic analysis**

534 Bacteroids were extracted from 14 dpi frozen nodules<sup>6</sup>, while bacterial culture samples were  
535 collected as above, and the bacterial pellets were resuspended in -20°C acetone and lysed by  
536 sonication. Protein solubilization, dosage, digestion (trypsin 2% w/w) and solid phase  
537 extraction (using Phenomenex polymeric C18 column) were performed as described before<sup>52</sup>.  
538 Peptides from 800 ng of proteins were analyzed by LC-MS/MS with a Q Exactive mass

539 spectrometer (Thermo Electron) coupled to a nanoLC Ultra 2D (Eksigent) using a  
540 nanoelectrospray interface (non-coated capillary probe, 10  $\mu$  i.d.; New Objective). Peptides  
541 were loaded on a Biosphere C18 trap-column (particle size: 5  $\mu$ m, pore size: 12 nm, inner/outer  
542 diameters: 360/100  $\mu$ m, length: 20 mm; NanoSeparations) and rinsed for 3 min at 7,5 $\mu$ l minute  
543 of 2% Acetonitrile (ACN), 0,1% Formic acid (FA) in water. Peptides were then separated on a  
544 Biosphere C18 column (particle size: 3  $\mu$ m, pore size: 12 nm, inner/outer diameters: 360/75  
545  $\mu$ m, length: 300 mm; NanoSeparations) with a linear gradient from 5% of 0,1% FA in ACN  
546 (buffer B) and 95% of 0,1% FA in Water (buffer A) to 35% of buffer B and 65% of buffer A  
547 in 80 min at 300nl/min followed by a rinsing step at 95% of buffer B and 5% of buffer A for 6  
548 min and a regeneration step with parameters of the start of the gradient for 8 min. peptide ions  
549 were analyzed using Xcalibur 2.1 software in data dependent mode with the following  
550 parameters: (I) full ms was acquire for the 400-1400 m/z range at a resolution of 70000 with an  
551 AGC target of  $3.10^6$ ; (ii) MS<sup>2</sup> scan was acquired at a resolution of 17500 with an agc target of  
552  $5.10^4$ , a maximum injection time of 120 ms and an isolation window of 3 m/z. The normalized  
553 collision energy was set to 27. MS<sup>2</sup> scan was performed for the eight most intense ions in  
554 previous full MS scan with an intensity threshold of  $1.10^3$  and a charge between 2 and 4.  
555 Dynamic exclusion was set to 50s. After conversion to mzXML format using msconvert  
556 (3.0.3706)<sup>53</sup>, data were searched using X!tandem (version 2015.04.01.1)<sup>54</sup> against the  
557 USDA110 reannotated protein database and a homemade database containing current  
558 contaminants. In a first pass trypsin was set to strict mode and cysteine carbamidomethylation  
559 as a fixed modification and methionine oxidation, protein N-terminal acetylation with or  
560 without protein N-terminal methionine excision, N-terminal glutamine and  
561 carbamidomethylated cysteine deamidation, N-terminal glutamic dehydration as potential  
562 modifications. In a refine pass, Semi enzymatic peptides were allowed. Proteins inference was  
563 performed using X!TandemPipeline (version 3,4,3)<sup>55</sup>. A protein was validated with an E-value

564  $< 10^{-5}$  and 2 different peptides with an E-value  $< 0.05$ . Protein from contaminant database  
565 (*Glycine max* proteins and unpublished *Aeschynomene* Expressed Sequence Tags) were  
566 removed after inference. Proteins were quantified using the spectral counting method<sup>56</sup>. To  
567 discriminate differentially accumulated proteins (DAPs), ANOVA analysis was performed on  
568 the spectral counts and proteins were considered DAP when p-value  $< 0.05$ .

569

#### 570 **Metabolomic analysis**

571 Metabolites and cofactors were extracted from lyophilized nodules and analyzed by GC-  
572 MS and LC-MS respectively according to Su et al. (2016)<sup>57</sup>.

573

#### 574 **Plant biomass and nitrogen fixation analysis**

575 Dry mass of shoot, root and nodules was measured, and shoot-root mass ratio was  
576 calculated. The mass gain per g of dry nodule was calculated as the difference between total  
577 mean masses of the plants of interest and of the non-inoculated plants, divided by the mean  
578 mass of nodules. Thirty plants were used per condition. Nitrogenase activity was assessed by  
579 Acetylene Reduction Assay (ARA) on ten plants per condition as previously described<sup>31</sup>. The  
580 elemental analysis of leaf carbon and nitrogen content was performed as described in reference  
581 18.

582

#### 583 **Analysis of *B. diazoefficiens* USDA110 regulons and stimulons**

584 Gene sets defined as regulons and stimulons were collected from the literature and the  
585 regulons/stimulons were considered as activated/repressed when  $\geq 40\%$  of the corresponding  
586 genes were DEG in a host plant as compared to the culture condition.

587

#### 588 **Comparison of orthologous gene expression between *B. diazoefficiens* USDA110 and**

589 *Bradyrhizobium* sp. ORS285



590 The list of orthologous genes between USDA110 and ORS285 was determined using the  
591 Phyloprofile tool of the MicroScope-MAGE platform<sup>58</sup>, with identity threshold of 60%,  
592 maxLrap > 0 and minLrap > 0.8. The RNA-seq data from reference 17 and those of this study  
593 were used to produce heatmaps, for the genes displaying FDR < 0.01 (*A. afraspera* vs. YM),  
594 using R (v3.6.3) and drawn using pheatmap (v1.0.12) coupled with kohonen (v3.0.10) for gene  
595 clustering using the Self Organizing Maps (SOM) method. The DEG in both organisms (*A.*  
596 *afraspera* vs YM) were plotted for USDA110 and ORS285.

597

### 598 **Analysis of TBD features**

599 Bacteroids were extracted from 14 dpi nodules and analyzed using a CytoFLEX S  
600 (Beckman-Coulter)<sup>31</sup>. For ploidy and live/dead analyses, samples were stained with propidium  
601 iodide (PI, ThermoFisher, 50 µg.mL<sup>-1</sup> final) and Syto9 (ThermoFisher, 1.67 µM final). PI  
602 permeability was assessed over time on live bacteria. *Bradyrhizobium* sp. ORS285.pMG103-  
603 *nptII-GFP*<sup>30</sup> and *B. diazoefficiens* USDA110 sYFP2-1<sup>59</sup> strains were used to distinguish  
604 bacteroid from debris during flow cytometry analysis. For each time point, the suspension was  
605 diluted 50 times for measurement in the flow-cytometer. The percentage of bacteroids  
606 permeable to PI was estimated as the ratio of PI-positive over total bacteroids (GFP/YFP  
607 positive). Heat-killed bacteroids were used as positive control to identify the PI-stained  
608 bacteroid population.

609 For bacteroid viability assays, nodules were collected and surface sterilized (1 min NaClO  
610 0.4%, 1 min 70% ethanol, two washes in sterile water). Bacteroids were subsequently prepared  
611 as previously described<sup>31</sup> and serially diluted and plated (five µl per spot) in triplicate on YM  
612 medium containing 50 µg.mL<sup>-1</sup> carbenicillin. Colony-forming units (cfu) were counted five  
613 days post plating and divided by the total nodule mass.

614 Bacterial cell shape, length and width were determined using confocal microscopy image  
615 analysis. Bacteroid extracts and stationary phase bacteria cultures were stained with 2.5 nM Syto9  
616 for 10 minutes at 37°C and mounted between slide and coverslip. Bacteria imaging was  
617 performed on a SP8 laser scanning confocal microscope (Leica microsystems) equipped with  
618 hybrid detectors and a 63x oil immersion objective (Plan Apo, NA: 1.4, Leica). For each  
619 condition, multiple z-stacks (2.7µm width, 0.7 µm step) were automatically acquired  
620 (excitation: 488 nm; collection of fluorescence: 520-580 nm).

621 Prior to image processing, each stack was transformed as a maximum intensity projection  
622 using ImageJ software (<https://imagej.nih.gov/ij/>). Bacteria detection was performed with  
623 MicrobeJ (<https://www.microbej.com/>)<sup>60</sup>. First, bacteria were automatically detected on every  
624 image using an intensity based thresholding method with a combination of morphological filters  
625 (area: 1-20 µm<sup>2</sup>; length: 1 µm-∞; width: 0.5-1.3 µm) and every object was fitted with a “Rod-  
626 shaped” bacteria model. To ensure high data quality every image was manually checked to  
627 remove false positive (mainly plant residues) and include rejected objects (mainly fused  
628 bacteria). Then the morphology measurements and figures were directly extracted from  
629 MicrobeJ. ORS285 in culture and in symbiosis with *A. afraspera* were used as references for  
630 the analysis of TBD features.

631

### 632 **Western blot analysis**

633 Detection of NifH by western blotting was performed using a commercial polyclonal  
634 antibody against a NifH peptide (Agrisera) respectively. The western blotting was carried out  
635 as previously described<sup>61</sup> using bacterial exponential (OD<sub>600nm</sub> = 0.5) and stationary (OD<sub>600nm</sub> >  
636 2.5) phase cultures as well as 14 dpi nodule-extracted bacteroids.

637

### 638 **Acknowledgments**

639 The authors would like to thank Dora Latinovics for production and sequencing of the RNA-  
640 seq libraries and Mélisande Blein-Nicolas for her advices regarding the statistical analysis of  
641 the proteomic dataset. Q.N. and F.L. were supported by a PhD fellowship from the Université  
642 Paris-Sud. The present work has benefited from the core facilities of Imagerie-Gif  
643 (<http://www.i2bc.paris-saclay.fr>), member of IBiSA (<http://www.ibisa.net>), supported by  
644 ‘France-BioImaging’ (ANR-10-INBS-04–01), and the Labex ‘Saclay Plant Sciences’ (ANR-  
645 11-IDEX-0003-02). This work was funded by the Agence Nationale de la Recherche, grants n°  
646 ANR-13-BSV7-0013 and ANR-17-CE20-0011 and used resources from the National Office for  
647 Research, Development and Innovation of Hungary, grant n° 120120 to A.K.

648

#### 649 **Authors’ contribution**

650 QN, FL, PM, BGo and BA designed the work. QN, FL, AC, TB, MB, FGu, ES, ST and OP  
651 performed the experiments. QN, FL, MB, ES, YD, BGa, FGi, IN, AK, MZ, PM, BGo and BA  
652 analyzed the data. QN, FL, PM, BGo and BA wrote the paper.

653

#### 654 **References**

- 655 1. Erisman, J.W., Galloway, J.N., Seitzinger, S., Bleeker, A., Dise, N.B., Petrescu,  
656 A.M.R., et al. (2013) Consequences of human modification of the global nitrogen cycle.  
657 *Philos Trans R Soc B Biol Sci* **368**: 20130116–20130116.
- 658 2. Zhao, C., Liu, B., Piao, S., Wang, X., Lobell, D.B., Huang, Y., et al. (2017) Temperature  
659 increase reduces global yields of major crops in four independent estimates. *Proc Natl*  
660 *Acad Sci U S A* **114**: 9326–9331.
- 661 3. Oldroyd, G. (2013) Speak, friend, and enter: signalling systems that promote beneficial  
662 symbiotic associations in plants. *Nat Rev Microbiol* **11**: 252–263.

- 663 4. Gourion, B. and Alunni, B. (2018) Strain-specific symbiotic genes: A new level of  
664 control in the intracellular accommodation of rhizobia within legume nodule cells. *Mol*  
665 *Plant-Microbe Interact* **31**: 287–288.
- 666 5. Mergaert, P., Nikovics, K., Kelemen, Z., Maunoury, N., Vaubert, D., Kondorosi, A., et  
667 al. (2003) A novel family in *Medicago truncatula* consisting of more than 300 nodule-  
668 specific genes coding for small, secreted polypeptides with conserved cysteine motifs.  
669 *Plant Physiol* **132**: 161–73.
- 670 6. Mergaert, P., Uchiumi, T., Alunni, B., Evanno, G., Cheron, A., Catrice, O., et al. (2006)  
671 Eukaryotic control on bacterial cell cycle and differentiation in the rhizobium-legume  
672 symbiosis. *Proc Natl Acad Sci U S A* **103**: 5230–5235.
- 673 7. Van de Velde, W., Zehirov, G., Szatmari, A., Debreczeny, M., Ishihara, H., Kevei, Z.,  
674 et al. (2010) Plant peptides govern terminal differentiation of bacteria in symbiosis.  
675 *Science* **327**: 1122–1126.
- 676 8. Guefrachi, I., Nagymihaly, M., Pislariu, C.I., Van de Velde, W., Ratet, P., Mars, M., et  
677 al. (2014) Extreme specificity of NCR gene expression in *Medicago truncatula*. *BMC*  
678 *Genomics* **15**(1):712.
- 679 9. Czernic, P., Gully, D., Cartieaux, F., Moulin, L., Guefrachi, I., Patrel, D., et al. (2015)  
680 Convergent evolution of endosymbiont differentiation in Dalbergioid and Inverted  
681 Repeat-Lacking Clade legumes mediated by nodule-specific cysteine-rich peptides.  
682 *Plant Physiol* **169**: 1254–1265.
- 683 10. Alunni, B., and Gourion, B. (2016) Terminal bacteroid differentiation in the legume-  
684 rhizobium symbiosis: nodule-specific cysteine-rich peptides and beyond. *New Phytol*  
685 **211**: 411–417.

- 686 11. Montiel, J., Downie, J.A., Farkas, A., Bihari, P., Herczeg, R., Bálint, B., et al. (2017)  
687 Morphotype of bacteroids in different legumes correlates with the number and type of  
688 symbiotic NCR peptides. *Proc Natl Acad Sci U S A* **114**: 5041–5046.
- 689 12. Farkas, A., Maróti, G., Dürgo, H., Györgypal, Z., Lima, R.M., Folkl-Medzihradsky, K.,  
690 Kereszt, A., Mergaert, P., and Kondorosi, E. (2014) *Medicago truncatula* symbiotic  
691 peptide NCR247 contributes to bacteroid differentiation through multiple mechanisms.  
692 *Proc Natl Acad Sci U S A* **111**: 5183-5188.
- 693 13. Koch, M., Delmotte, N., Rehrauer, H., Vorholt, J.A., Pessi, G., and Hennecke, H. (2010)  
694 Rhizobial adaptation to hosts, a new facet in the legume root-nodule symbiosis. *Mol*  
695 *Plant-Microbe Interact* **23**: 784–790.
- 696 14. Renier, A., Maillet, F., Fardoux, J., Poinso, V., Giraud, E., and Nouwen, N. (2011)  
697 Photosynthetic *Bradyrhizobium* Sp. strain ORS285 synthesizes 2-O-methylfucosylated  
698 lipochitooligosaccharides for nod gene-dependent interaction with *Aeschynomene*  
699 plants. *Mol Plant Microbe Interact* **24**: 1440–7.
- 700 15. Ledermann, R., Bartsch, I., Müller, B., Wülser, J., and Fischer, H.M. (2018) A  
701 functional general stress response of *Bradyrhizobium diazoefficiens* is required for early  
702 stages of host plant infection. *Mol Plant-Microbe Interact* **31**: 537–547.
- 703 16. Barrière, Q., Guefrachi, I., Gully, D., Lamouche, F., Pierre, O., Fardoux, J., et al. (2017)  
704 Integrated roles of BclA and DD-carboxypeptidase 1 in *Bradyrhizobium* differentiation  
705 within NCR-producing and NCR-lacking root nodules. *Sci Rep* **7**: 1–13.
- 706 17. Lamouche, F., Gully, D., Chaumeret, A., Nouwen, N., Verly, C., Pierre, O., et al. (2019)  
707 Transcriptomic dissection of *Bradyrhizobium* sp. strain ORS285 in symbiosis with  
708 *Aeschynomene* spp. inducing different bacteroid morphotypes with contrasted symbiotic  
709 efficiency. *Environ Microbiol.* **21**: 3244–3258.

- 710 18. Lamouche, F., Chaumeret, A., Guefrachi, I., Barrière, Q., Pierre, O., Guérard, F., et al.  
711 (2019) From intracellular bacteria to differentiated bacteroids: transcriptome and  
712 metabolome analysis in *Aeschynomene* nodules using the *Bradyrhizobium* sp. ORS285  
713 *bclA* mutant. *J. Bacteriol* **201**: e00191-19.
- 714 19. Andrews, M., Raven, J.A., Lea, P.J., and Sprent, J.I. (2006) A role for shoot protein in  
715 shoot-root dry matter allocation in higher plants. *Ann Bot* **97**: 3-10.
- 716 20. Collier, R., and Tegeder, M. (2012) Soybean ureide transporters play a critical role in  
717 nodule development, function and nitrogen export. *Plant J.* **72**: 355-67.
- 718 21. Ross, E.J.H.H., Kramer, S.B., and Dalton, D.A. (1999) Effectiveness of ascorbate and  
719 ascorbate peroxidase in promoting nitrogen fixation in model systems. *Phytochemistry*  
720 **52**: 1203–1210.
- 721 22. Bashor, C.J. and Dalton, D.A. (1999) Effects of exogenous application and stem  
722 infusion of ascorbate on soybean (*Glycine max*) root nodules. *New Phytol* **142**: 19–26.
- 723 23. Sallet, E., Gouzy, J., and Schiex, T. (2014) EuGene-PP: a next-generation automated  
724 annotation pipeline for prokaryotic genomes. *Bioinformatics* **30**: 2659–61.
- 725 24. Bittner, A.N., Foltz, A., and Oke, V. (2007) Only one of five *groEL* genes is required  
726 for viability and successful symbiosis in *Sinorhizobium meliloti*. *J Bacteriol* **189**: 1884–  
727 9.
- 728 25. Lardi, M., Murset, V., Fischer, H. M., Mesa, S., Ahrens, C. H., Zamboni, N. et al. (2016)  
729 Metabolomic Profiling of *Bradyrhizobium diazoefficiens*-Induced Root Nodules  
730 Reveals Both Host Plant-Specific and Developmental Signatures. *Int J Mol Sci* **17**(6) :  
731 815.
- 732 26. Thede, G. L., Arthur, D. C., Edwards, R. A., Buelow, D. R., Wong, J. L., Raivio, T. L.,  
733 & Glover, J. N. (2011) Structure of the periplasmic stress response protein CpxP.  
734 *Journal Bacteriol* **193**(9): 2149–57.

- 735 27. diCenzo, G.C., Zamani, M., Checcucci, A., Fondi, M., Griffiths, J.S., Finan, T.M., and  
736 Mengoni, A. (2018) Multi-disciplinary approaches for studying rhizobium – legume  
737 symbioses. *Peer J* **cjm-2018-0377**.
- 738 28. Teufel, R., Mascaraque, V., Ismail, W., Voss, M., Perera, J., Eisenreich, W., et al. (2010)  
739 Bacterial phenylalanine and phenylacetate catabolic pathway revealed. *Proc Natl Acad*  
740 *Sci U S A* **107**: 14390–5.
- 741 29. Okazaki, S., Nukui, N., Sugawara, M., and Minamisawa, K. (2004) Rhizobial strategies  
742 to enhance symbiotic interactions: rhizobitoxine and 1-aminocyclopropane-1-  
743 carboxylate deaminase. *Microb. Environ* **19**: 99–111.
- 744 30. Bonaldi, K., Gargani, D., Prin, Y., Fardoux, J., Gully, D., Nouwen, N., et al. (2011)  
745 Nodulation of *Aeschynomene afraspera* and *A. indica* by photosynthetic  
746 *Bradyrhizobium* sp. strain ORS285: the Nod-dependent versus the Nod-independent  
747 symbiotic interaction. *Mol Plant-Microbe Interact* **24**: 1359–1371.
- 748 31. Guefrachi, I., Pierre, O., Timchenko, T., Alunni, B., Barrière, Q., Czernic, P., et al.  
749 (2015) *Bradyrhizobium* BclA is a peptide transporter required for bacterial  
750 differentiation in symbiosis with *Aeschynomene* legumes. *Mol Plant-Microbe Interact*  
751 **28**: 1155–1166.
- 752 32. Crespo-Rivas, J.C., Guefrachi, I., Mok, K.C., Villaécija-Aguilar, J.A., Acosta-Jurado,  
753 S., Pierre, O., et al. (2016) *Sinorhizobium fredii* HH103 bacteroids are not terminally  
754 differentiated and show altered O-antigen in nodules of the Inverted Repeat-Lacking  
755 Clade legume *Glycyrrhiza uralensis*. *Environ Microbiol* **18**: 2392–2404.
- 756 33. Montiel, J., Szűcs, A., Boboescu, I.Z., Gherman, V.D., Kondorosi, E., and Kereszt, A.  
757 (2016) Terminal bacteroid differentiation is associated with variable morphological  
758 changes in legume species belonging to the Inverted Repeat-Lacking Clade. *Mol Plant*  
759 *Microbe Interact* **29**(3): 210-9.

- 760 34. Price, P.A., Tanner, H.R., Dillon, B.A., Shabab, M., Walker, G.C., and Griffitts, J.S.  
761 (2015) Rhizobial peptidase HrrP cleaves host-encoded signaling peptides and mediates  
762 symbiotic compatibility. *Proc Natl Acad Sci U S A* **112**: 15244–15249.
- 763 35. Tiricz, H., Szücs, A., Farkas, A., Pap, B., Lima, R.M., Maróti, G., et al. (2013)  
764 Antimicrobial nodule-specific cysteine-rich peptides induce membrane depolarization-  
765 associated changes in the transcriptome of *Sinorhizobium meliloti*. *Appl Environ*  
766 *Microbiol* **79**: 6737–6746.
- 767 36. Kulkarni, G., Busset, N., Molinaro, A., Gargani, D., Chaintreuil, C., Silipo, A., et al.  
768 (2015) Specific hopanoid classes differentially affect free-living and symbiotic states of  
769 *Bradyrhizobium diazoefficiens*. *MBio* **6**: 1–9.
- 770 37. Oono, R., Schmitt, I., Sprent, J.I., and Denison, R.F. (2010) Multiple evolutionary  
771 origins of legume traits leading to extreme rhizobial differentiation. *New Phytol* **187**(2):  
772 508-20
- 773 38. Karmakar, K., Kundu, A., Rizvi, A.Z., Dubois, E., Severac, D., Czernic, P., et al. (2019)  
774 Transcriptomic analysis with the progress of symbiosis in ‘crack-entry’ legume *Arachis*  
775 *hypogaea* highlights its contrast with ‘infection thread’ adapted legumes. *Mol Plant-*  
776 *Microbe Interact* **32**(3):271-285.
- 777 39. Kereszt, A., Mergaert, P., Montiel, J., Endre, G., and Kondorosi, E. (2018) Impact of  
778 plant peptides on symbiotic nodule development and functioning. *Front Plant Sci.*  
779 **9**:1026
- 780 40. Trujillo, D.I., Silverstein, K.A.T., and Young, N.D. (2019) Nodule-specific PLAT  
781 domain proteins are expanded in the *Medicago* lineage and required for nodulation. *New*  
782 *Phytol* **222**: 1538–1550.



- 783 41. Gourion, B., Sulser, S., Frunzke, J., Francez-Charlot, A., Stiefel, P., Pessi, G., et al.  
784 (2009) The PhyR- $\sigma$ EcfG signalling cascade is involved in stress response and symbiotic  
785 efficiency in *Bradyrhizobium japonicum*. *Mol Microbiol* **73**: 291–305.
- 786 42. Roux, B., Rodde, N., Jardinaud, M.F., Timmers, T., Sauviac, L., Cottret, L., et al. (2014)  
787 An integrated analysis of plant and bacterial gene expression in symbiotic root nodules  
788 using laser-capture microdissection coupled to RNA sequencing. *Plant J* **77**(6):817-37.
- 789 43. Sen, D. and Weaver, R.W. (1981) A comparison of nitrogen-fixing ability of peanut,  
790 cowpea and siratro plants nodulated by different strains of *Rhizobium*. *Plant Soil* **60**:  
791 317–319.
- 792 44. Oono, R. and Denison, R.F. (2010) Comparing symbiotic efficiency between swollen  
793 versus nonswollen rhizobial bacteroids. *Plant Physiol* **154**: 1541–1548.
- 794 45. Kazmierczak, T., Nagymihaly, M., Lamouche, F., Barriere, Q., Guefrachi, I., Alunni,  
795 B., et al. (2017) Specific host-responsive associations between *Medicago truncatula*  
796 accessions and *Sinorhizobium* strains. *Mol. Plant Microbe Interact.* 30:399–409.
- 797 46. Lamouche, F., Bonadé-Bottino, N., Mergaert, P., and Alunni, B. (2019) Symbiotic  
798 efficiency of spherical and elongated bacteroids in the *Aeschynomene-Bradyrhizobium*  
799 symbiosis. *Front. Plant Sci* **10**: 377.
- 800 47. Regensburger, B. and Hennecke, H. (1983) RNA polymerase from *Rhizobium*  
801 *japonicum*. *Arch Microbiol* **135**: 103–109.
- 802 48. Giraud, E., Hannibal, L., Fardoux, J., Verméglio, A., and Dreyfus, B. (2000) Effect of  
803 *Bradyrhizobium* photosynthesis on stem nodulation of *Aeschynomene sensitiva*. *Proc*  
804 *Natl Acad Sci U S A* **97**: 14795–14800.
- 805 49. Chapelle, E., Alunni B, Malfatti P, Solier L, Pedron J, Kraepiel Y, Van Gijsegem F.  
806 (2015) A straightforward and reliable method for bacterial *in planta* transcriptomics:

- 807 application to the *Dickeya dadantii/Arabidopsis thaliana* pathosystem. *Plant J* **82**:352–  
808 362.
- 809 50. Azani, N., Babineau, M., Bailey, C.D., Banks, H., Barbosa, A.R., Pinto, R.B., *et al.*  
810 (2017) A new subfamily classification of the Leguminosae based on a taxonomically  
811 comprehensive phylogeny – The Legume Phylogeny Working Group (LPWG). *Taxon*  
812 **66**: 44–77.
- 813 51. Brottier, L., Chaintreuil, C., Simion, P., Scornavacca, C., Rivallan, R., Mournet, P., *et*  
814 *al.* (2018) A phylogenetic framework of the legume genus *Aeschynomene* for  
815 comparative genetic analysis of the Nod-dependent and Nod-independent symbioses.  
816 *BMC Plant Biol* **18**: 333.
- 817 52. Langella O, Valot B, Jacob D, Balliau T, Flores R, Hoogland C, Joets J, Zivy M. (2013)  
818 Management and dissemination of MS proteomic data with PROTIcDb: example of a  
819 quantitative comparison between methods of protein extraction. *Proteomics*  
820 **13**(9):1457-66.
- 821 53. Kessner D, Chambers M, Burke R, Agus D, Mallick P. (2008) ProteoWizard: open  
822 source software for rapid proteomics tools development. *Bioinformatics* **24**(21):2534-6.
- 823 54. Craig R, Beavis RC. (2004) TANDEM: matching proteins with tandem mass spectra.  
824 *Bioinformatics* **20**(9):1466-7.
- 825 55. Langella O, Valot B, Balliau T, Blein-Nicolas M, Bonhomme L, Zivy M. (2017)  
826 X!TandemPipeline: A tool to manage sequence redundancy for protein inference and  
827 phosphosite identification. *J Proteome Res.* **16**(2):494-503.
- 828 56. Delmotte N, Mondy S, Alunni B, Fardoux J, Chaintreuil C, Vorholt JA, Giraud E,  
829 Gourion B. (2014) *Int J Mol Sci.* **15**(3):3660-70.
- 830 57. Su, F., Gilard, F., Guérard, F., Citerne, S., Clément, C., Vaillant-Gaveau, N., and  
831 Dhondt-Cordelier, S. (2016) Spatio-temporal responses of *Arabidopsis* leaves in

- 832 photosynthetic performance and metabolite contents to *Burkholderia phytofirmans*  
833 PsJN. *Front Plant Sci* **7**: 1–15.
- 834 58. Médigue, C., Calteau, A., Cruveiller, S., Gachet, M., Gautreau, G., Josso, A., *et al.*  
835 (2019) MicroScope-an integrated resource for community expertise of gene functions  
836 and comparative analysis of microbial genomic and metabolic data. *Brief Bioinform* **20**:  
837 1071-1084.
- 838 59. Ledermann, R., Bartsch, I., Remus-Emsermann, M.N., Vorholt, J.A., and Fischer, H.M.  
839 (2015) Stable fluorescent and enzymatic tagging of *Bradyrhizobium diazoefficiens* to  
840 analyze host-plant infection and colonization. *Mol Plant-Microbe Interact* **28**: 959–967.
- 841 60. Ducret, A., Quardokus, E. M., & Brun, Y. V. (2016). MicrobeJ, a tool for high  
842 throughput bacterial cell detection and quantitative analysis. *Nature Microbiology*, **1**(7),  
843 16077.
- 844 61. Beroual, W., and Biondi, E.G. (2019) A new factor controlling cell envelope integrity  
845 in Alphaproteobacteria in the context of cell cycle, stress response and infection. *Mol*  
846 *Microbiol.* **111**(3):553-555.

847

## 848 **Figure legends**

849

850 **Figure 1. The non-adapted symbiotic couple formed by *Bradyrhizobium diazoefficiens***  
851 **USDA110 and the NCR-producing plant *Aeschynomene afraspera* displays suboptimal**  
852 **nitrogen fixation and nodule metabolic dysfunction.** A. Phylogenetic ML tree of a selection  
853 of plant species based on *matK* nucleotide sequences. Red branches indicate clades of legumes  
854 plants inducing terminal bacteroid differentiation. Blue boxes indicate the distantly-related host  
855 plants used in this study. Bootstrap values are mentioned in green on each node of the tree. B,C.  
856 General aspect of the plants and nodule sections (inlays) displaying the red coloration of

857 leghaemoglobin of *G. max* (B) and *A. afraspera* (C) at 14 dpi. Scale bars: 5 cm (plants) and 1  
858 mm (nodules). D, E. Nitrogen fixation activity determined by acetylene reduction assay (D) and  
859 gain in biomass attributable to the symbiosis (E) of 14 dpi plants. F. Whole-nodule metabolome  
860 determined by GC/MS or LC/MS at 14 dpi. Histograms show the average value of the relative  
861 metabolite concentration of four biological replicates. Letters represent significant differences  
862 after ANOVA and post hoc Tukey tests ( $p < 0.05$ ). GM: *G. max* bacteroids, AA: *A. afraspera*  
863 bacteroids, USDA: *B. diazoefficiens* USDA110, ORS: *Bradyrhizobium sp.* ORS285.

864

865 **Figure 2. Experimental setup and general description of the transcriptomics and**  
866 **proteomics dataset.** A. Experimental setup displaying the three biological conditions of this  
867 study. B. Principal component analysis of the proteomics and transcriptomics datasets. C. Venn  
868 diagram representing the overlap between differentially expressed genes (DEGs,  $FDR < 0.01$   
869 &  $|LFC| > 1.58$ ) and differentially accumulated proteins (DAPs,  $FDR < 0.05$ ) in at least one  
870 comparison and among the population of detected proteins. D. Pearson correlation coefficient  
871 ( $r$ ) distribution between transcriptomic and proteomic datasets based on DAPs only (red) or  
872 DAPs that are also DEGs (green). E. Heatmaps and hierarchical clustering of the 815 DAPs  
873 and the corresponding transcriptomic expression values. The heatmaps show the standard score  
874 ( $z$ -score) of assigned spectra and DESeq2 normalized read counts, respectively. The color-  
875 coded scale bars for the normalized expression and value of Pearson correlation coefficient of  
876 the genes are indicated below the heatmap. YM: Yeast-Mannitol culture, GM: *G. max*  
877 bacteroids, AA: *A. afraspera* bacteroids.

878

879 **Figure 3: Symbiosis and host-specific functions that display congruency between**  
880 **transcriptomics and proteomics** A. Heatmap with SOM clustering displaying bacterial  
881 functions that are commonly DAP and DEG *in planta* in both host plants as compared to the

882 culture reference. B. Heatmap displaying bacterial functions that are commonly DEG and DAP  
883 in one host as compared to the other (upper panel: *A. afraspera* > *G. max*; lower panel: *G. max*  
884 > *A. afraspera*). In panels A-B, data are presented as log 2 of DESeq2 normalized read counts  
885 (RNA-seq) or spectral counting (Proteomics). YM: Yeast-Mannitol culture, GM: *G. max*  
886 bacteroids, AA: *A. afraspera* bacteroids.

887

888 **Figure 4: Expression pattern of *B. diazoefficiens* USDA110 and *Bradyrhizobium* sp.**  
889 **ORS285 orthologous genes *in planta* and in culture.** A. Heatmap after SOM clustering of all  
890 the orthologous genes of USDA110 and ORS285 obtained with Phyloprofile. Values present  
891 the *in planta* LFC calculated after the read counts of the culture control versus *A. afraspera* 14  
892 dpi nodules. B. Heatmaps of the orthologous genes after filtering on the FDR (< 0.01) values.  
893 Selected genes are highlighted for each class of interest. C. Dot plot of the orthologous genes  
894 that are DEG (FDR < 0.01 and |LFC| > 1.58) *in planta* (ie. in *A. afraspera* nodules) in both  
895 strains. The red dashed line is for the linear regression and the blue envelope shows a 0.95  
896 confidence interval of the linear regression.

897

898 **Figure 5. *B. diazoefficiens* USDA110 displays atypical bacteroid differentiation features**  
899 **in *A. afraspera* nodules.** A. Average cell shape of free-living bacteria and bacteroids  
900 determined by MicrobeJ (900 < n < 21 000). B. DNA content of USDA110 bacteroids extracted  
901 from soybean and *A. afraspera* determined by flow cytometry. C. Assessment of the  
902 permeability of USDA110 and ORS285 free-living cells and bacteroids 20 min after PI  
903 treatment. \*: wilcoxon test, p-value < 0.01. Five biological replicates were performed for  
904 bacteroids and two for free-living bacteria. D. Viability of soybean and *A. afraspera* extracted  
905 bacteroids at 14 dpi. Asterisks point out significant differences according to a wilcoxon test. \*:  
906 p-value < 0.05; \*\*: p-value < 0.01. Data are representative of 10 independent plants.

907

908 **Supplementary figure and table legends**

909

910 **Figure S1. Nitrogen and carbon content in aerial parts of the plants were determined by**  
911 **elemental analysis.** GM: *G. max*, AA: *A. afraspera*, ORS: inoculated by *Bradyrhizobium* sp.  
912 ORS285, USDA: inoculated by *B. diazoefficiens* USDA110, NI: Non-inoculated plants.

913

914 **Figure S2. Nutritional status of 14 dpi plants determined by the shoot/root mass ratios.**  
915 AA: *A. afraspera*, ORS: inoculated by *Bradyrhizobium* sp. ORS285, USDA: inoculated by *B.*  
916 *diazoefficiens* USDA110, NI: Non-inoculated plants. Letters represent significant differences  
917 after t-test or ANOVA and post hoc Tukey tests ( $p < 0.05$ ).

918

919 **Figure S3. Overview of the 129 quantified metabolites in *G. max* and *A. afraspera* whole**  
920 **nodules elicited by *B. diazoefficiens* USDA110 or *Bradyrhizobium* sp. ORS285.** Heatmap  
921 and hierarchical clustering of the 129 metabolites that were quantified either by gas- (GC-MS)  
922 or liquid-chromatography (LC-MS) coupled to mass spectrometry. Gm: *G. max*, Aa: *A.*  
923 *afraspera*, O: inoculated by *Bradyrhizobium* sp. ORS285, U: inoculated by *B. diazoefficiens*  
924 USDA110.

925

926 **Figure S4. General overview of the datasets using COG classification.** Repartitions of the  
927 assigned spectra (left panel) and normalized reads (right panel) among COG classes in the three  
928 conditions (blue: bacterial culture, ocher: *B. diazoefficiens* USDA110 in *G. max* nodules, green:  
929 *B. diazoefficiens* USDA110 in *A. afraspera* nodules).

930

931 **Figure S5. Western blot analysis of selected USDA110 proteins in culture and in**  
932 **bacteroids.** NifH protein were analyzed by western blots on purified USDA110 bacteroids  
933 extracted from soybean and *A. afraspera* nodules 14 dpi. Exponential and stationary phase  
934 cultures were used as controls.

935

936 **Figure S6. Analysis of cellular differentiation using automated morphometry.** A, B, C &  
937 D. Parameters were quantified by image analysis of syto9 stained bacteria and bacteroids using  
938 MicrobeJ. The process from raw images (A), segmentation (B), object detection (C) and  
939 measurements (D) is depicted with these four panels. E. Cell area. F. Cell width. G. Cell length.

940

941 **Figure S7. Kinetic analysis of bacterial membrane permeability.** Kinetics of propidium  
942 iodide uptake assays (reflecting membrane permeability) from which data presented in Figure  
943 5C were extracted. The PI permeability was measured by flow cytometry over 60 min after  
944 treatment on *A. afraspera* nodule extracted USDA110 (AaU) or ORS285 (AaO) bacteroids and  
945 *G. max* extracted USDA110 bacteroids at 14 dpi (GmU). Exponential phase bacterial culture  
946 of USDA110 and ORS285 where used as controls. Each dot represent three independent  
947 measures and error bars represent the standard deviation of the samples.

948

949 **Table S1. Genome annotation, transcriptomic and proteomic data of *B. diazoefficiens***  
950 **USDA110 generated in this study.** Description of proteomic and transcriptomic data of  
951 USDA110 related conditions. DESeq2 normalized reads, false discovery rate (FDR) values as  
952 well as log<sub>2</sub> fold change (LFC) are used to describe transcriptomic data. On the other side,  
953 spectral counting (SC) along with related statistical indicators, Tukey statistical test result and  
954 p-value depict the proteomic data.

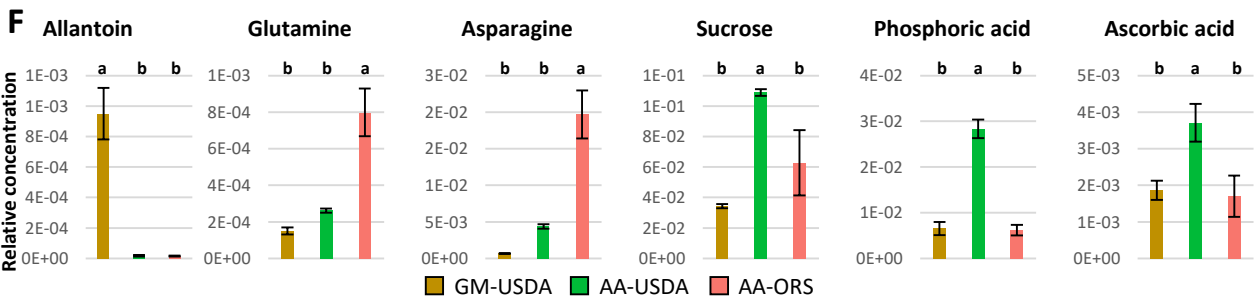
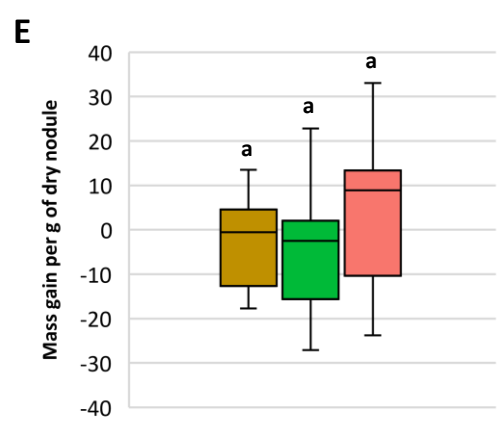
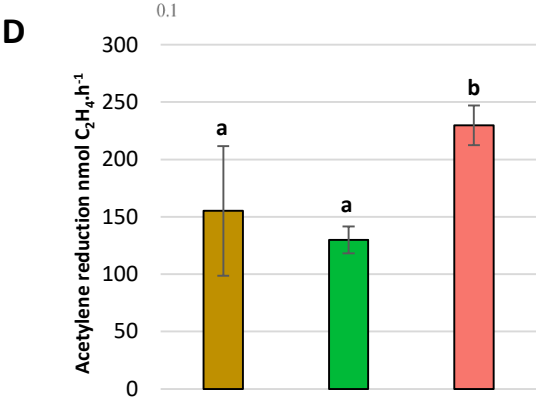
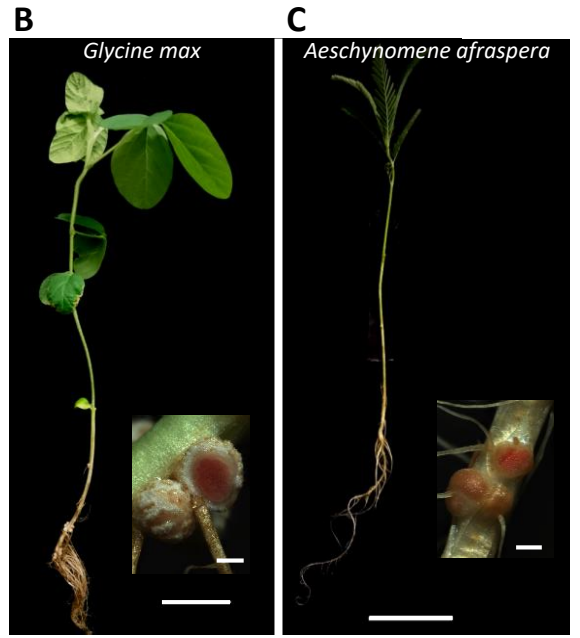
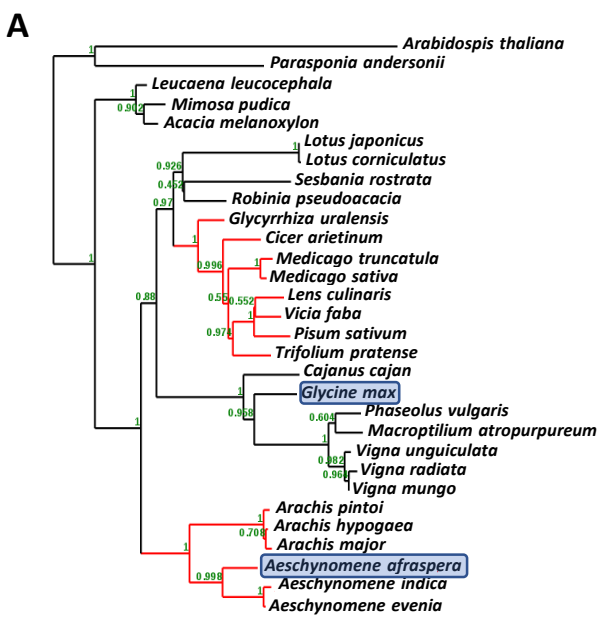
955

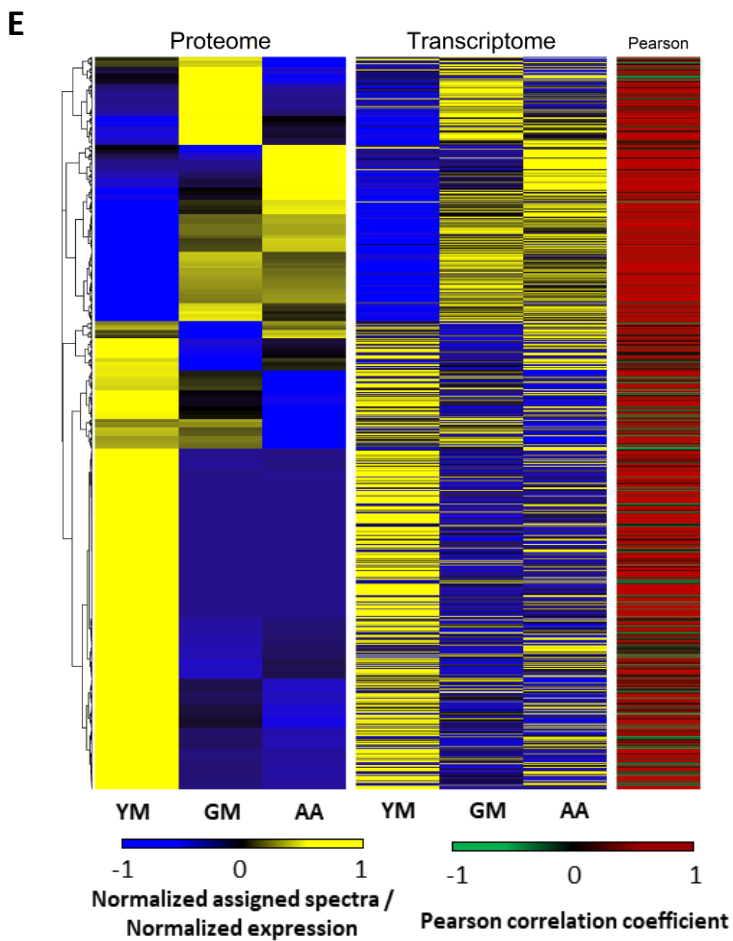
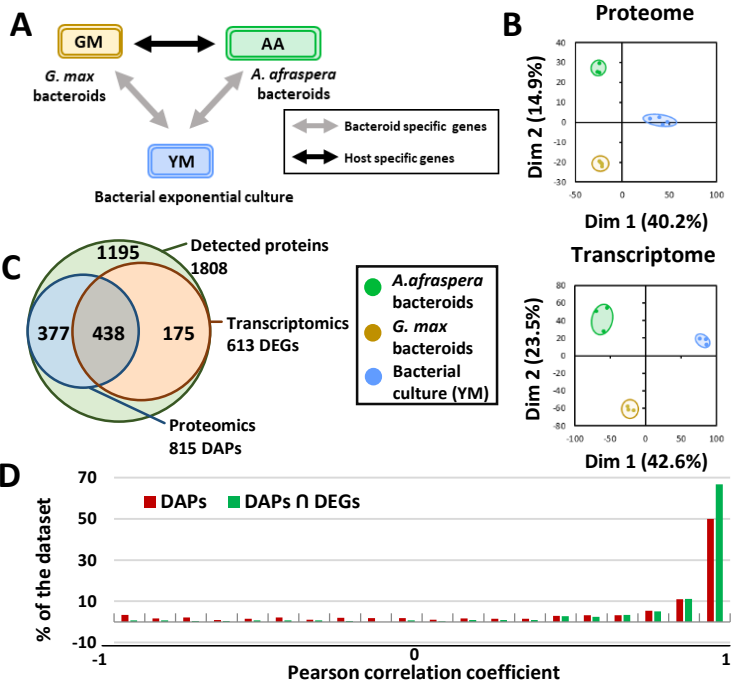
956 **Table S2. Expression analysis of selected *B. diazoefficiens* USDA110 regulons and**  
957 **stimulons.** Detailed analysis of the previously determined regulons and stimulons of USDA110  
958 based on our transcriptomic data. A given regulon/stimulon was considered differentially  
959 regulated when  $\geq 40\%$  of the corresponding genes were differentially expressed in our  
960 conditions.

961

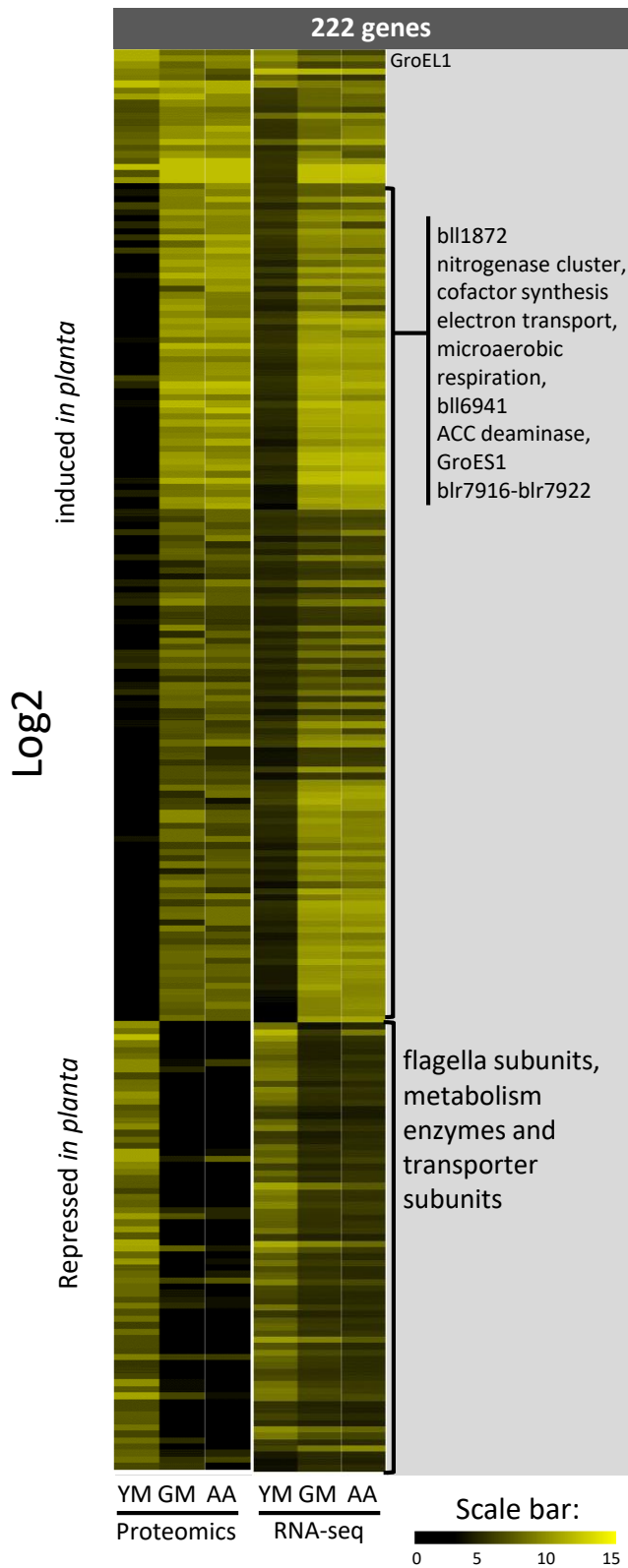
962 **Table S3. List of the 3725 orthologous genes shared by *B. diazoefficiens* USDA110 and**  
963 ***Bradyrhizobium* sp. ORS285 with their corresponding expression level in rich medium and**  
964 **in *A. afraspera* nodules.** This dataset was obtained after a Phyloprofile analysis on Mage  
965 Microscope website and was used to generate the Figure 4. Normalized read counts are shown  
966 together with the corresponding LFC and FDR as determined by DESeq2.







**A.**



**B.**

